Spatial distributions of droplet size and velocity in air heated spray

Measured by interferometric laser imaging technique

by

Goro Takeuchi [(1)], Tatsuya Kawaguchi [(2)], Koichi Hishida [(1)], Masanobu Maeda [(1)] and Martin Sommerfeld [(3)]

[(1)] Keio University
Department of System Design Engineering Faculty of Science and Technology
Hiyoshi 3-13-1, Kohoku-ku, Yokohama, Japan

E-Mail: takeuchi@mh.sd.keio.ac.jp

[(2)] Tokyo Institute of Technology
Department of Mechanical and Control Engineering
O-okayama 2-12-1, Meguro-ku, Tokyo, Japan

[(3)] Visiting professor at Keio University
Martin-Luther-University of Halle
Department of Engineering Science, Institute of Process Engineering
D-06099 Halle (Saale), Germany

ABSTRACT

The behaviour of a water spray centrally injected into a swirling annular jet (initial outer diameter 56.5mm) was studied experimentally. Two flow conditions were compared, namely a non-heated and a heated airflow issuing into quiescent air (Figure 1). The water spray was produced using a full cone nozzle mounted centrally into the injection pipe. The instantaneous spatial distribution of droplet size and velocity was measured applying the interferometric laser imaging technique (ILIDS). The circular out-of-focus images were first optically squeezed for allowing an easier and more reliable analysis of the images. The fringe spacing, which is proportional to the droplet diameters, was determined by discrete Fourier transform and a Gaussian interpolation technique. The droplet velocity was obtained from the displacement of the squeezed images recorded or two subsequent images. The results demonstrate that the interaction of the spray with the swirling free jet flow and the established recirculation zone results in bimodal droplet size distributions for both the non-heated and heated case (Figure 2). As expected, droplet evaporation in the heated case yields a faster decrease of the mean droplet size along the spray than for the non-heated case.

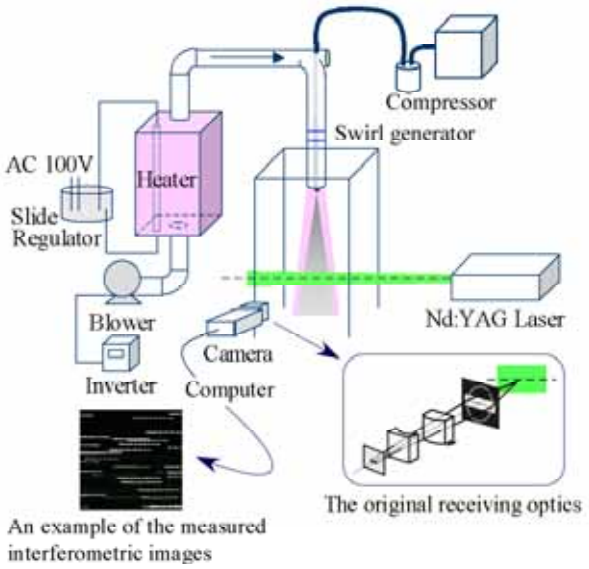

Fig. 1. Schematics of experimental set-up and interferometric laser imaging technique

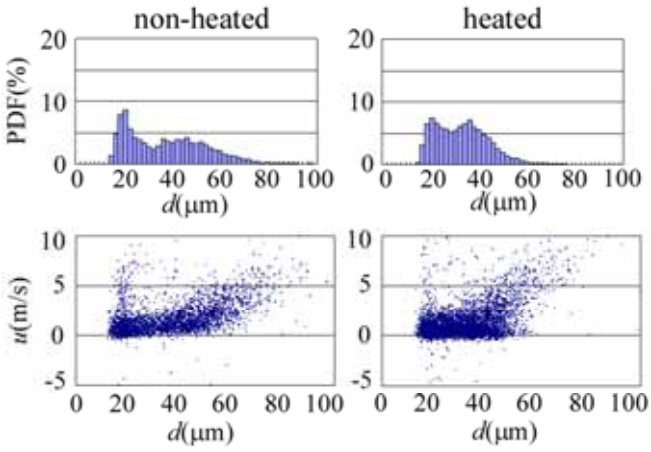

Fig. 2. Size distributions and correlation maps between diameter and axial velocity at (z,r)=(75,0)

1. INTRODUCTION

For understanding the transient spray, not only the averaged size and velocity distributions of droplets are of importance, but also the instantaneous properties of individual droplets are required to understand the unsteady behavior of droplets and flow structure, and to evaluate heat and mass transport processes. Interferometric laser imaging for droplet sizing is a method that provides an instantaneous spatial distribution of droplet size by analyzing the out-of-focus image of droplets (Glover *et al.* 1995). The angular phase difference of the external reflection from the surface and the direct refraction through the droplet allows to derive a relation between fringe spacing and droplet size. The measurement accuracy depends on the estimation of the size of the out-of-focus image and the fringe spacing.

In the present technique, an advanced imaging technique and accelerated data processing by a fast computer system was developed whereby the circular images with fringes are optically squeezed into linear images by defocusing horizontally and focusing vertically (Maeda *et al.* 2000, 2002, Kawaguchi *et al.* 2002). The squeezing technique reduced the involved noise and the signal to noise ratio of the interferogram becomes much better than that of conventional technique as a consequence. Moreover, the optical compression technique can eliminate distorted or inclined interference signal resulting from wall reflection and multiple scattering. The preferential fringe acquisition technique provides genuine interferential signals that give the diameter of particles. The signal processing procedure for the determination of the droplet diameter requires only one-dimensional information of the fringe spacing which was evaluated by discrete Fourier transform and Gaussian interpolation technique of the power spectrum. The accurate diameter determination enables to identify the particles in successive images and to measure the velocity vectors of each droplet even from images of denser sprays. The direct digital acquisition of images and the fully automated image processing software provide high quality data for up to six hundred droplets in a frozen image of 10mm x10mm. Furthermore, the size determination from the scattering pattern of droplets is not affected by the refractive index by the temperature fluctuation (Kawaguchi *et al.* 2003). i.e. the diameter coefficient that relates the size of particle and fringe separation is almost independent of the refractive index.

In this study, the planar droplet sizing technique has been applied for a spray issuing into a heated swirling flow. Swirling two-phase flows are encountered in a variety of forms in many engineering applications. In combustion systems the special features of swirling flows are used to establish high mixing rates between the fuel and the swirling air stream and to enhance flame stability. To improve the understanding of swirling flow, a number of studied have been carried out in the past. The particle dispersion characteristics in a confined swirling flow were studied by Sommerfeld *et al.* (1991, 1993) using a phase-Doppler technique and numerical predictions. Their results demonstrate the behaviour of different sized particles in a complex flow and the spatial change of the particle-size distribution throughout the flow field. Hardalupas *et al.* (1990, 1994) studied the velocity-size correlation of droplets in a liquid-fuelled swirl burner. Their results demonstrate the different behavior of different sized droplets in a swirling free jet emanating from a quarl-type burner nozzle.

2. TEST FACILITY

The test facility for the experimental studies is shown in Figure 3. It consists of an inverter-controlled blower with variable flow rate, a heater array followed by a pipe system, a swirl generator and a measurement section with quadratic cross-section (500 × 500mm) and a length of 1000mm. Eight coil-fin-electric-heaters were embedded in the heating chamber. The maximum output of each heater was 500W with AC 100V power supply. The input voltage of heaters was adjusted by a slide regulator to change the temperature of the airflow. The geometry of the inflow pipe is shown in Figure 4. The internal diameter of the pipe is 56.5mm and the centrally mounted nozzle holder has an outer diameter of 13.8mm. For generating the annular swirling airflow, a swirler is mounted 150mm above the pipe exit which consists of four swirl vanes. The inclination of the swirl vanes with respect to the vertical axis is 60°. A Delavan type B solid cone nozzle was used with the injection pressure of 0.8MPa, the flow rate of $5.3\times10^{-7}m^3$/sec and the working fluid of water.

The flow conditions for the non-heated and heated case are shown in table 1. The velocity of the airflow was measured by a laser-Doppler anemometry. For comparing non-heated and heated condition the mean air velocity was kept almost constant. The temperature was measured by a thermo-couple. Figure 5 shows the temperature distribution within the measurement section at various cross-sections downstream of the pipe exit for the heated case. These measurements were of course performed without the spray. The mean air inlet temperature for the heated case was about 373K. Due to the mixing of the heated swirling jet with the surrounding air the temperature rapidly decays along the measurement section.

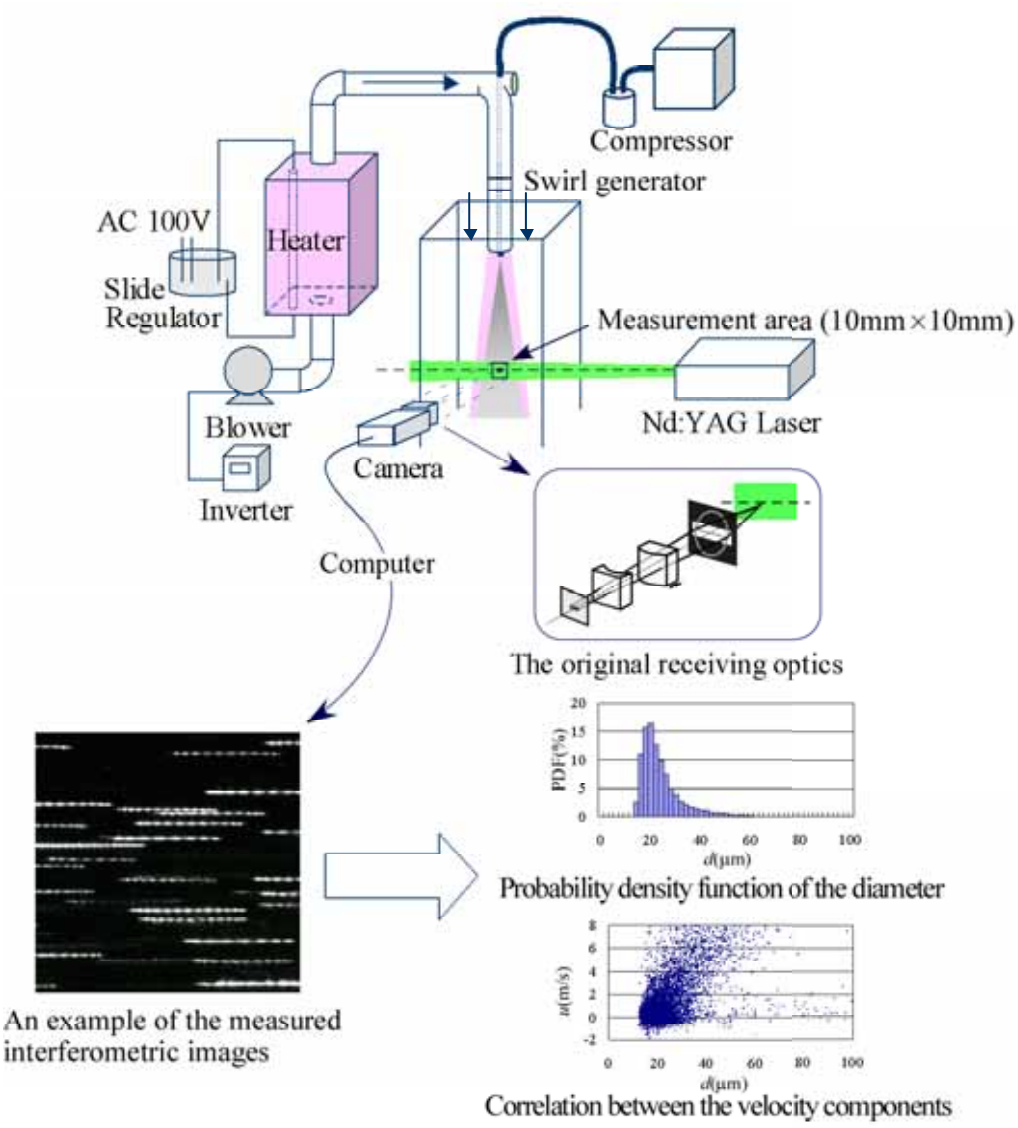

Fig. 3. Schematics of experimental set-up and interferometric laser imaging technique

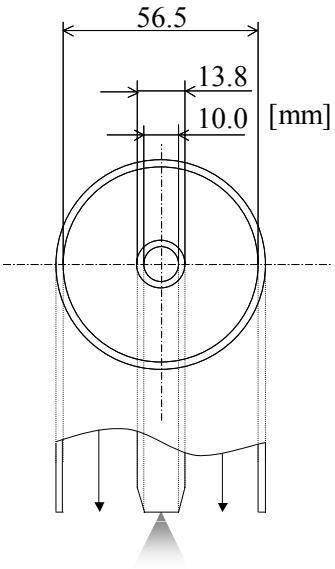

Fig. 4. Schematic drawing of inlet pipe with dimensions

Table 1. Flow conditions

	non-heated	heated
$\overline{u}_{gas}$	1.2m/s	1.3m/s
$\overline{T}_{gas}$	298K	373K
$\dot{m}_{gas}$	330g/s	280g/s
Re_{gas} (obtain with $D = 56.5$mm)	42000	45000

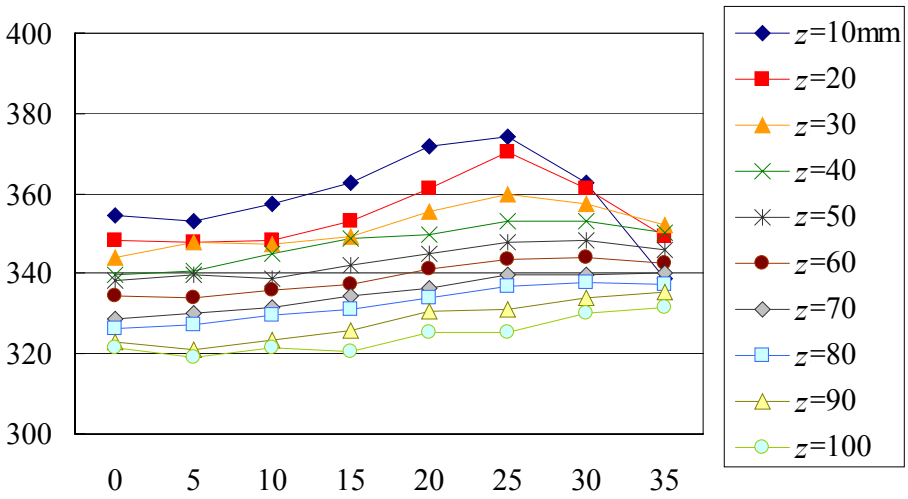

Fig. 5. Temperature profiles along the measurement for the heated case without droplets

3. MEASUREMENT TECHNIQUE

When a spherical droplet is illuminated by laser light, the intensity of the reflected and refracted light from the droplet are stronger than that of higher order refractions in the forward-scatter region between about 30 to 80deg. On the focal image plane, two spots are observed as glare points (Van de Hulst and Wang 1991). Although the distance between the glare points gives the particle size, it is difficult to evaluate the size thereby because of the lack of spatial resolution of conventional receiving equipment. On a non-focal plane, the two rays interfere with each other and a parallel interferogram is observed. ILIDS measures the diameter of a spherical transparent particle on the basis of the inter-fringe separation or the number of fringes within the interferogram. Girasole *et al* (2000) calculated the adequate defocus distance and concluded that a sufficient defocusing distance is required for the far-field condition of the receiving optics. Van de Hulst (1957) reported that a reasonable agreement between the geometric analysis and the full Lorenz-Mie theory was obtained for the size parameter $\pi d/\lambda > 20$ for the condition that the refractive index of the droplets differed significantly from its surrounding and that rays close to grazing incidence and those close to the rainbow angles were not involved. For the present optical arrangement of $\lambda = 532$nm, the lower limit of the measured droplet diameter is 2μm resulting from the geometric optical analysis.

The angular inter-fringe spacing is simply proportional to the droplet diameter and independent of the absolute light intensity (Hesselbacher *et al* 1991, Toth *et al* 1991). It is easily derived by noting the phase difference between the reflection and refraction from a single droplet. The relation between particle diameter d and the number of fringes N is given by the following equation based on geometric optical analysis.

$$d = \frac{2\lambda N}{\alpha} \frac{1}{\cos\frac{\theta}{2} + \frac{m\sin\frac{\theta}{2}}{\sqrt{m^2 + 1 - 2m\cos\frac{\theta}{2}}}} \tag{1}$$

where λ is the wavelength of the laser light source and m is the relative refractive index of the liquid droplet. θ and α are scattering and collecting angle, respectively. The fringe number N is equivalent to α divided by the angular inter-fringe spacing.

Figure 6 shows the dependence of the measured droplet diameter on the refractive index, resulting from Eq. 1 for a scattering angle of 73deg. The calculated diameter, d, was normalized by the reference diameter, d_{ref}, of a water droplet in an atmospheric temperature. The result shows that 1% increase or decrease of the relative refractive results in a measurement error of less than 0.06% in diameter.

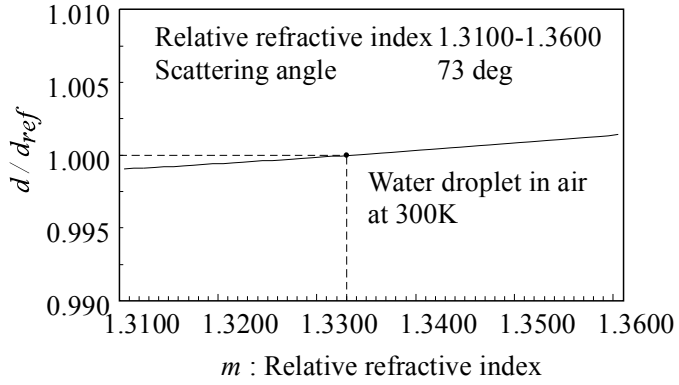

Fig. 6. Refractive index dependency of a measured diameter.

A conventional interferometric laser imaging technique has the difficulty in discriminating the images of particles due to the overlapping of the circular interferograms in high particle concentration regions. An interferential signal within the fringe overlapping region is not a simple summation of a sinusoid and therefore the image processing of the overlapped interferogram becomes complicated or even impossible.

Figure 7 illustrates the fundamental optical arrangement of the advanced interferometric laser imaging technique (Maeda *et al.* 2000, 2002, Kawaguchi *et al.* 2002). A pair of cylindrical lenses was placed between the imaging plane and the objective lens in order to project the horizontal out-of-focus images on a vertically focused plane. The cylindrical lens can be moved along the optical axis of the receiving optics that enables to adjust the degree of horizontal defocusing. By using the squeezing optical system, such confusing image overlapping as in the conventional ILIDS techniques had been drastically reduced.

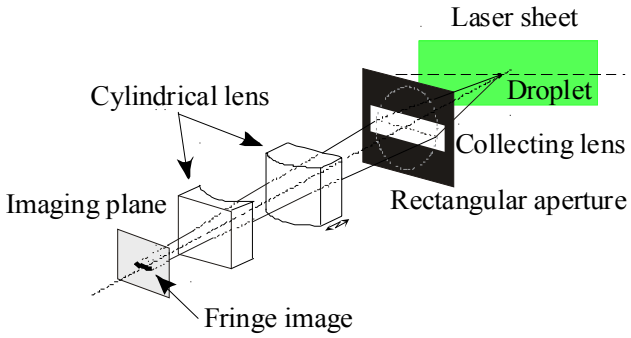

Fig. 7. Optical arrangement of the advanced interferometric laser imaging technique.

After the sequential acquisition of the images with linear interferograms, a fully automated image processing of the interferograms was carried out by an original code on a personal computer. The software identifies the individual fringe images and determines their location within the image. The interferogram can be detected by scanning the captured image horizontally that gives a similar signal as the Doppler burst signal for the LDV technique. The concept of the signal processing procedure for the evaluation of fringe spacing is the same as that of FFT based LDV/PDA processing techniques by which the accurate frequency is calculated with the adjusted Gaussian fitting method for the discrete Fourier power spectrum (Kobashi *et al.* 1990). The interpolation technique is effective in the reduction of bias errors to less than 0.2% for the fundamental frequency. The resultant resolution of the measured fringe count, which is directly proportional to the diameter, becomes much higher than the simple peak determination of the power spectrum. The accurate diameter determination by the interpolation technique contributes to the particle tracking and velocity calculation since the precise diameter information, which conventional particle tracking techniques does not survey, enables us to find the corresponding particles between the image pairs. For the determination of the droplet velocities a particle tracking technique was employed (Maeda *et al.* 2002). For this purpose the centroids of the squeezed droplet images were obtained for two subsequent images (Figure 8).

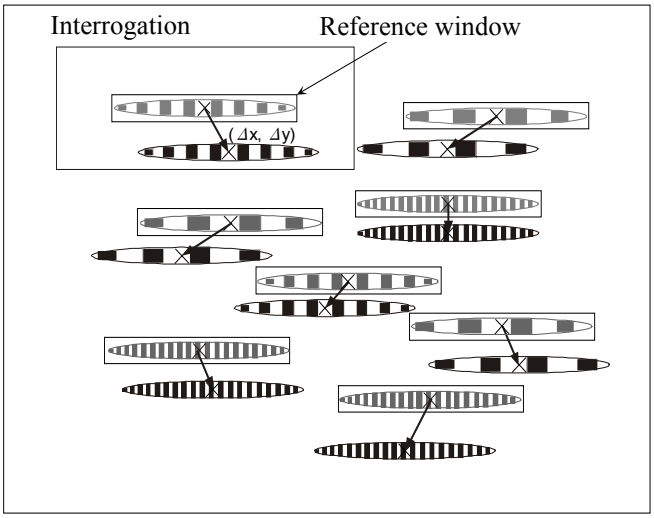

Fig. 8. Particle tracking technique for the determination of the droplet velocities

The measurement equipment consisted of a pulsed laser, transmitting and receiving optics, CCD camera and personal computer with frame grabber. The light source was a dual pulsed Nd:YAG laser with 532nm wavelength, the maximum output power was 120mJ/pulse, the repetition frequency was up to 15Hz, the time interval between laser pulses was set to 6μs. The thickness of the laser sheet was 0.5mm within the test section. Circularly polarized light was used for a better discrimination between interferogram and background. The imaging device was a digital CCD camera with 1008×1018 pixels, each pixel has a 10bit grayscale level. The size of the measuring area was set to 10mm×10mm, which depends on the magnification ratio of the receiving optics. The distance from the objective lens to the test section was 180mm and the collecting angle was 5deg. The scattering angle was set to 73deg to receive high visibility interference by equalizing the intensity of reflection and refraction.

4. RESULTS AND DISCUSSION

A Snapshot of the steady spray in a non-heated swirling flow is shown in Figure 9. Measurements of the droplet size and velocity were conducted at 15 locations within the spray where the axial locations are z =25,45,75,105mm and the radial locations are r = 0, 10, 20, 30mm (at z=25mm, r=30mm, there are almost no droplet). At each measuring location 1430 pairs of the images were taken to obtain the information of droplets that exist in a 10mm×10mm measuring area.

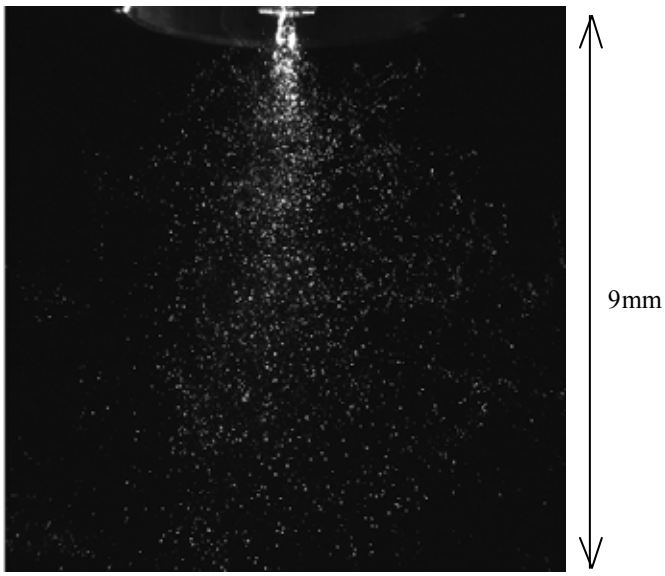

Fig. 9. Snapshot of a steady spray in a swirling flow

The probability density functions of the droplet diameter for the non-heated case are shown in Figure 10. Along the center of the spray, the number of the larger droplets increases compared to the smaller ones. Thereby, a bimodal droplet size distribution develops. This is a result of the interaction of the spray with the central recirculation region, causing the smaller droplets to be radially transported outward since they are able to respond to the airflow. The larger droplets penetrate the recirculation region to a large extent (Sommerfeld and Qiu 1993). At the same axial location, the number of smaller droplets increases at the edge of the spray. This is a result of the fact that the smaller droplets follow the swirling flow and are carried away from the central region toward the edge of the spray.

Figure 11 shows the correlation maps between the droplet diameter and axial velocity for the non-heated case. Near the nozzle the droplets are fast up to about 10m/s. Along the spray core, smaller droplets are decelerated rather fast, whereas the inertia of the larger droplets is associated with a slower decrease of their axial velocity. Far downstream of the spray nozzle and at the edge of the spray, there exists almost no correlation between the axial droplet velocity and their size, indicating that all droplets move at about the same velocity. The negative droplet velocities found within the spray are the result of the droplet interaction with the central recirculation region. A higher probability for such negative velocities is found in a region 25-45mm downstream of the nozzle exit and between r=10-20mm, of course the smaller droplets have higher negative velocities. This observation is in accordance with the droplet trajectory calculations introduced by Sommerfeld and Qiu (1993). If small droplets enter centrally the recirculation region, they are decelerated and transported upward torwards the nozzle exit while moving radially outward due to the centrifuging effect. Hence, also the number of the droplets near the center of the spray decreases along the spray.

The size distributions an the centre line of the spray comparing the non-heated and heated case are shown in Figure 12. Droplet evaporation in the heated case yields a faster decrease of the mean droplet size along the spray than for the non-heated case. Also for the heated case a bimodal droplet size distribution develops within the recirculation zone. Figure 14 shows profiles of the Sauter mean diameter and the arithmetic mean diameter of droplets in the radial and axial direction, respectively. The droplet transport processes in a swirling flow described above cause a decrease of the droplet diameters from the centre line towards the edge of the spray (Figure 14 left). As expected, the droplet mean diameters are smaller for the heated case. Along the spray centre line the arithmetic mean droplet diameter increases due to the radial transport of the smaller droplets (Figure 14 right). The Sauter mean diameter first decreases, reaches a minimum and then increases again. This indicates that the droplet size distribution initially becomes more narrow and then broadens again. In the heated case the minimum of the SMD is located further downstream of the spray nozzle exit. Also the mean diameters are smaller for the heated case due to droplet evaporation.

Figure 13 compares the correlation maps between the droplet diameter and axial velocity for the non-heated and heated case. In the heated case the droplets have a somewhat higher velocity than in the non-heated case and also the correlation between size and velocity is strange. This might be associated with a slightly higher liquid velocity at the nozzle exit, since the water may be heated when flowing through the nozzle holder.

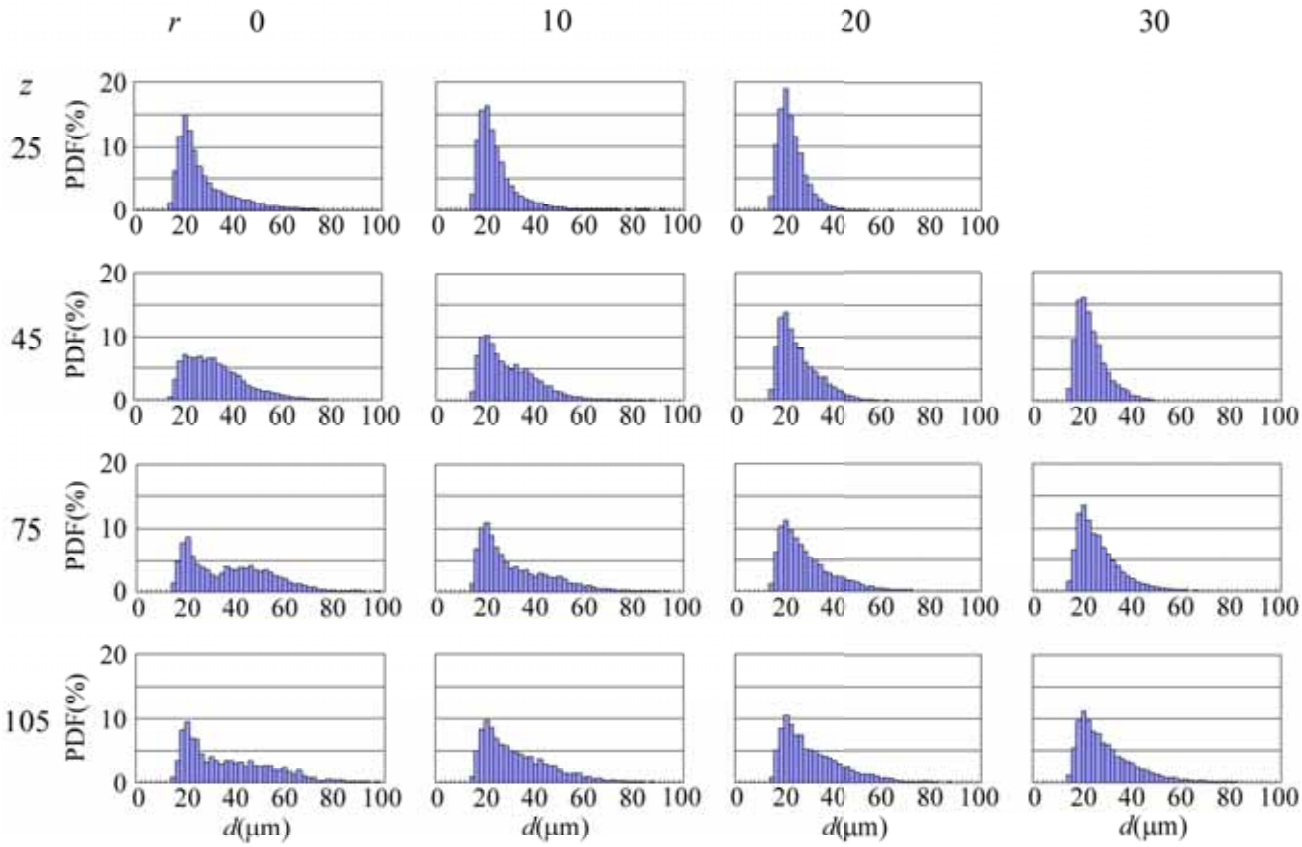

Fig. 1□ □robability density f□nctions of the droplet diameter for the non-heated

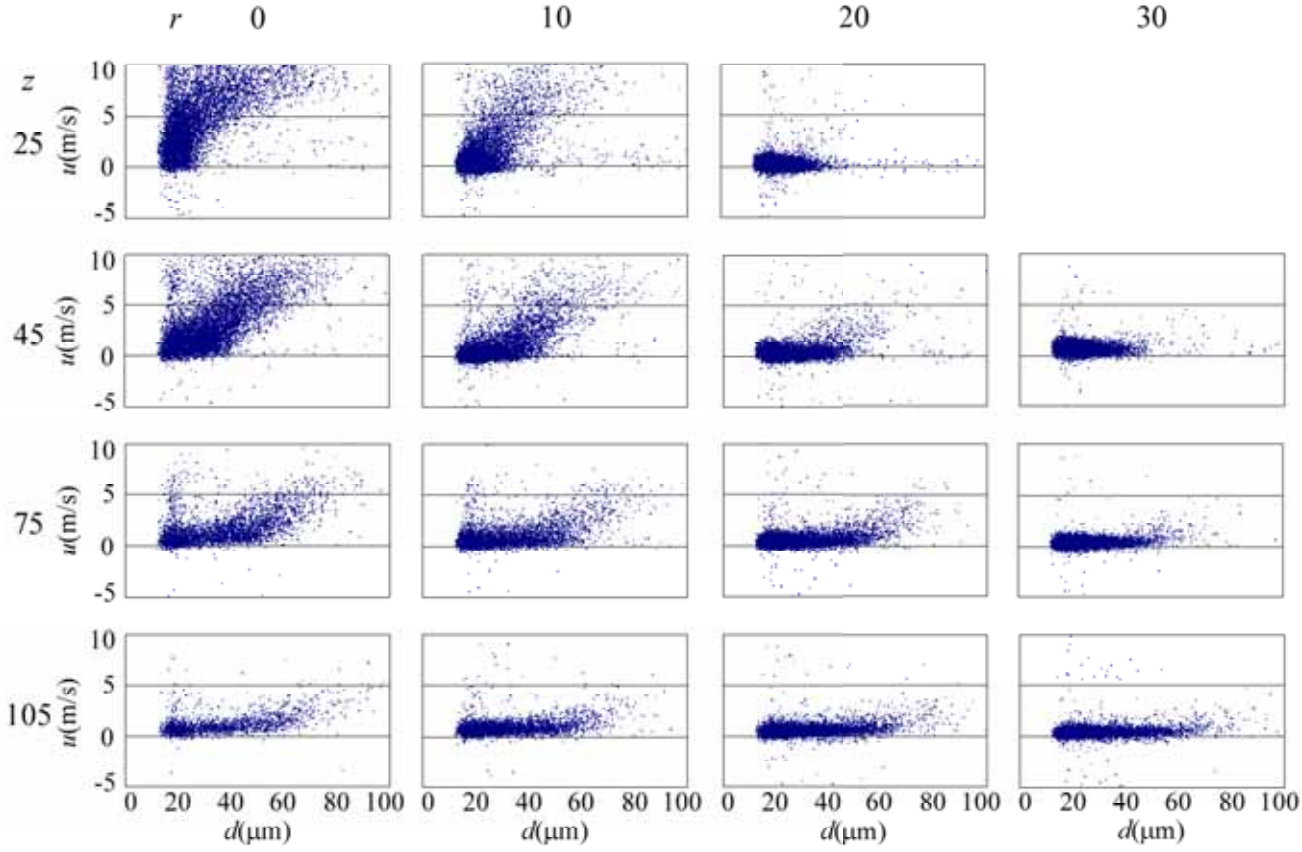

Fig. 11. Correlation maps between the axial velocity component, and the droplet size for the non-heated case

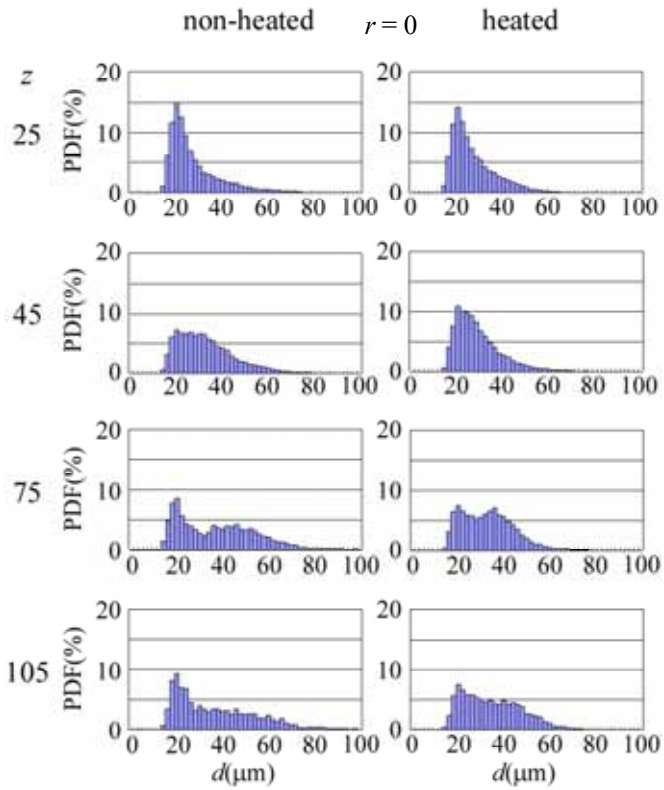

Fig. 12. Droplet size distributions comparing The non-heated and the heated cases

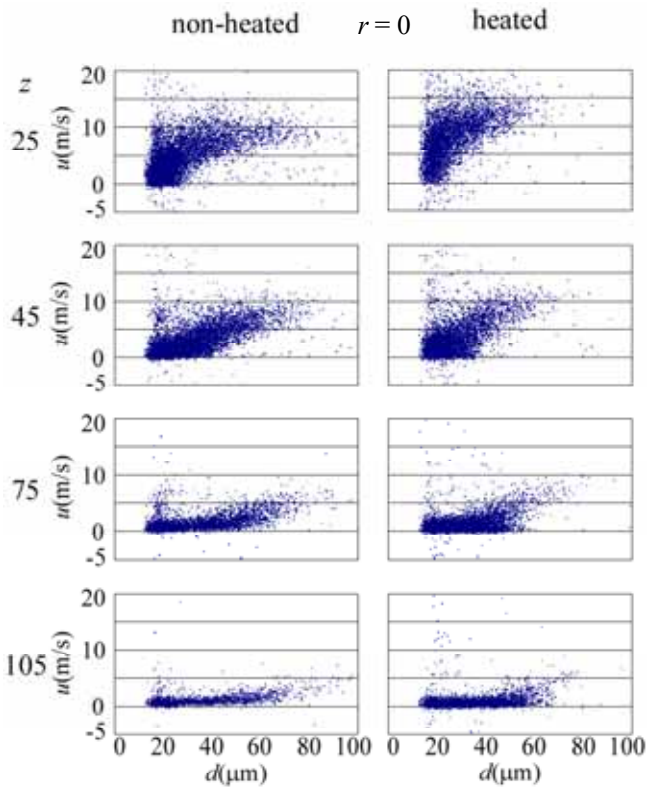

Fig. 13. Correlation maps between the diameter and the axial velocity

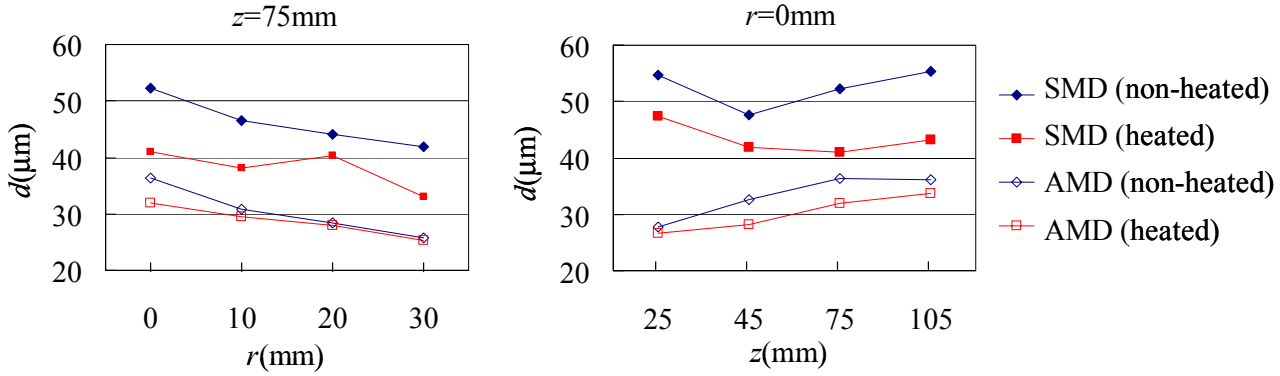

Fig. 14. Sauter and Arithmetic mean diameters of droplets (i.e. SMD and AMD) in the radial direction at z=75mm (left) and along the centre line of the spray (right)

5. SUMMARY

The behaviour of a water spray centrally injected into a swirling annular jet has been studied by applying interferometric laser imaging technique. Two flow conditions were compared, namely a non-heated and a heated airflow issuing into quiescent air. The results demonstrate that the interaction of the spray with the swirling free jet flow and the established recirculation zone results in bimodal droplet size distributions for both the non-heated and heated case. As expected, droplet evaporation in the heated case yields a faster decrease of the arithmetic mean droplet size along the spray than for the non-heated case. The distribution of the Sauter diameter along the spray shows a distinct minimum for both cases. This implies that the width of the droplet size distribution is first decreasing. Further studies will be performed for different swile numbers as sell as air injection temperatures.

REFERENCES

Girasole T., Ren K.F., Lebrun D., Gouesbet G. and Gréhan G. (2000), "Particle imaging sizing: GLMT simulations" *J. Visualization*, 3, 195-202

Glover A.R., Skippon S.M. and Boyle R.D. (1995), "Interferometric Laser Imaging for Droplet Sizing: A Method for Droplet-Size Measurement in Sparse Spray Systems", *Appl. Opt.*, 34, 8409-8421

Hardalupas, Y., Taylor, A.M.K.P. and Whitelaw, J.H. (1990), "Velocity and size characteristics of liquid-fuelled flames stabilized by a swirl burner", *Proc. R. Soc. Lond.*, A 428, 129-155

Hardalupas, Y., Taylor, A.M.K.P. and Whitelaw, J.H. (1994), "Mass flux, mass fraction and concentration of liquid fuel in a swirl-stabilized flame", *Int. J. Multiphase Flow*, 20, 233-259

Hesselbacher K.H., Anders K. and Frohn A. (1991), "Experimental investigation of Gaussian beam effects on the accuracy of a droplet sizing method", *Appl. Opt.*, 30, 4930-4930

Kawaguchi T., Akasaka Y. and Maeda M. (2002), "Size measurements of droplets and bubbles by advanced interferometric laser imaging technique", *Meas. Sci. Technol.*, 13, 308-316

Kawaguchi T., Akasaka Y., Hishida K., Maeda M. (2003), "Planar Measurement of Local Characteristics of Impinging Spray on Heating Plate", *Proceedings of the 6th ASME-JSME Thermal Engineering Joint Conference*

Kobashi K., Hishida K. and Maeda M. (1990), "Measurement of fuel injector spray flow of IC engine by FFT based phase Doppler anemometer-an approach to the time series measurement of size and velocity", *Application of Laser Techniques to Fluid Mechanics*, Ed, S.R.J. Adrian *et al* (Berlin:+Springer) pp 268-287

Maeda M., Kawaguchi T. and Hishida K. (2000), "Novel interferometric measurement of size and velocity distribution of spherical particles in fluid flow", *Meas. Sci. Technol.*, 11, L13-L18

Maeda M., Akasaka Y. and Kawaguchi T. (2002), "Improvements of the interferometric technique for simultaneous measurement of droplet size and velocity vector field and its application to a transient spray", *Exp. Fluids*, 33, 125-134

Roth N., Anders K. and Frohn A. (1991), "Refractive-index measurement for the correction of particle sizing methods", *Appl. Opt.*, 30, 4960-4965

Sommerfeld, M. and Qiu, H.-H. (1991), "Detailed measurements in a swirling particulate two-phase flow by a phase-Doppler anemometer", *Int. J. Heat and Fluid Flow*, 12, 20-28

Sommerfeld, M. and Qiu, H.-H. (1993), "Characterization of particle-laden, confined swirling flows by phase-Doppler anemometry and numerical calculation", *Int. J. Multiphase Flow*, 19, 1093-1127

Van de Hulst H.C. (1957), *Light Scattering by Small Particles*, (Willey: New York)

Van de Hulst H.C. and Wang R.T. (1991), "Glare points", *Appl. Opt.*, 30, 4755-4763